

Variational determination of approximate bright matter-wave soliton solutions in anisotropic traps

T. P. Billam, S. A. Wrathmall, and S. A. Gardiner

Department of Physics, Durham University, Durham DH1 3LE, United Kingdom

(Dated: February 16, 2019)

We consider the ground state of an attractively-interacting atomic Bose-Einstein condensate in a prolate, cylindrically symmetric harmonic trap. If a true quasi-one-dimensional limit is realized, then for sufficiently weak axial trapping this ground state takes the form of a bright soliton solution of the nonlinear Schrödinger equation. Using analytic variational and highly accurate numerical solutions of the Gross-Pitaevskii equation we systematically and quantitatively assess how soliton-like this ground state is, over a wide range of trap and interaction strengths. Our analysis reveals that the regime in which the ground state is highly soliton-like is significantly restricted, and occurs only for experimentally challenging trap anisotropies. This result, and our broader identification of regimes in which the ground state is well-approximated by our simple analytic variational solution, are relevant to a range of potential experiments involving attractively-interacting Bose-Einstein condensates.

PACS numbers: 03.75.Lm 67.85.Bc

I. INTRODUCTION

Bright solitons are self-focusing, non-dispersive, particle-like solitary waves occurring in integrable systems [1, 2]. They behave in a particle-like manner, emerging from mutual collisions intact except for shifts in their position and relative phase. Bright soliton solutions of the one-dimensional nonlinear Schrödinger equation (NLSE) can be described analytically using the inverse scattering technique [3, 4] and are well-known in the context of focusing nonlinearities in optical fibers [4, 5]. Bright solitary matter-waves in an attractively interacting atomic Bose-Einstein condensate (BEC) represent an intriguing alternative physical realization [6–8]. In a mean-field description an atomic BEC obeys the Gross-Pitaevskii equation (GPE) [9], a three-dimensional NLSE. While in general non-integrable, in a homogeneous, quasi-one-dimensional (quasi-1D) limit the GPE reduces to the one-dimensional NLSE, thus supporting bright solitons [10–15].

Outside the quasi-1D limit the GPE continues to support bright solitary matter-waves. These exhibit many soliton-like characteristics and have been the subject of much experimental [6–8] and theoretical [16–29] investigation. Both bright solitons and bright solitary waves are excellent candidates for use in atom interferometry [30], as their coherence, spatial localization and soliton-like dynamics offer a metrological advantage in, e.g., the study of atom-surface interactions [7, 20]. Towards this end, proposals to phase-coherently split bright solitons and bright solitary waves using a scattering potential [27–29] and an internal state interference protocol [18], and to form soliton molecules [26] have been explored in the literature. However, while the dynamics and collisions of bright solitary waves have been explored in detail and have been shown to be soliton-like in three-dimensional (3D) parameter regimes [16–18], less attention has been directed at the question of exactly how soliton-like the ground state of the system is. In particular, the experimental feasibility of reaching the quasi-1D limit of an attractively-interacting BEC, and hence obtaining a highly soliton-like ground state, remains an area lacking a thorough quantitative exploration. Obtaining such a ground state, in addition to being interesting in

its own right, would be highly advantageous in experiments seeking to probe quantum effects beyond the mean-field description [27–29], and possibly to exploit the effects of macroscopic quantum superposition to enhance metrological precision [31, 32]. Similar concerns regarding adverse residual 3D effects in interferometric protocols prompted a recent perturbative study of residual 3D effects in highly anisotropic, repulsively-interacting BECs [33].

The potential instability to collapse of attractively-interacting BECs [34–43] is the key obstacle to realizing soliton-like behavior in a BEC. Previous studies of bright solitary wave dynamics, using variational and numerical solutions of partially-quasi-1D GPEs [12, 13, 21, 44] (reductions of the GPE to a 1D equation which retain some 3D character, in contrast to the full quasi-1D limit) and the 3D GPE [16–18, 34], have shown the collapse instability to be associated with non-soliton-like behavior. However, previous studies of bright solitary wave ground states have focused on identifying the critical parameters at which collapse occurs. Approaches used in these studies include partially-quasi-1D methods [12], variational methods using Gaussian [10, 11, 34] and soliton (sech) [34, 45] ansatzes, perturbative methods [46], and numerical solutions to the 3D GPE [34, 35, 42, 43, 45]. In the latter case, the collapse threshold parameters have been extensively mapped out for a range of trap geometries [42, 43].

In this paper we use analytic variational and highly accurate numerical solutions of the stationary GPE to systematically and quantitatively assess how soliton-like the ground state of an attractively-interacting BEC in a prolate, cylindrically symmetric harmonic trap is, over a wide regime of trap and interaction strengths. Beginning with previously-considered variational ansatzes based on Gaussian [10, 11, 34] and soliton [34, 45] profiles, we obtain new, analytic variational solutions for the GPE ground state. Comparing the soliton-ansatz variational solution to highly accurate numerical solutions of the stationary GPE, which we calculate over an extensive parameter space, gives a quantitative measure of how soliton-like the ground state is. In the regime where the axial and radial trap strengths dominate over the interactions, we show that the Gaussian ansatz variational solution gives an excellent ap-

proximation to the true ground state for all anisotropies; in this regime the ground state is not soliton-like. In the regime in which the interactions dominate over the axial, but *not* the radial, trap strength we demonstrate that the soliton-ansatz variational solution does approximate the true, highly soliton-like ground state. However, we show that the goodness of the approximation and the extent of this regime, where it exists at all, is highly restricted by the collapse instability; even at large anisotropies it occupies a narrow window adjacent to the regime where interactions begin to dominate over *all* trap strengths, leading to non-quasi-1D, non-soliton-like solutions and, ultimately, collapse.

Our results have substantial practical value for experiments using attractively-interacting BECs; primarily they define the challenging experimental regime required to realize a highly soliton-like ground state, which would be extremely useful to observe quantum effects beyond the mean-field description such as macroscopic superposition of solitons [27–29]. We note that bright solitary wave experiments to date have not reached this regime [6–8]. Secondly, our quantitative analysis of a wide parameter space provides a picture of the ground state in a wide range of possible attractively-interacting BEC experiments. In particular, it indicates the regimes in which a full numerical solution of the 3D GPE is well-approximated by one of our analytic variational solutions, which are significantly easier and less time-consuming to determine.

The remainder of the paper is structured as follows: After introducing the most general classical field Hamiltonian and stationary GPE in Section II, we begin by discussing the quasi-1D limit in Section III. In Section III A we define the dimensionless trap frequency γ ; in the quasi-1D limit this is the *only* free parameter, and all our results are expressed in terms of this quantity. Similarly, our variational ansatzes are motivated by the limiting behaviors of the solution in the quasi-1D case; in this case we define them as Gaussian and soliton profiles, parametrized by their axial lengths. In Sections III B and III C we find, analytically, the energy-minimizing axial lengths for each ansatz as a function of γ . Comparison of the resulting ansatz solutions to highly accurate numerical solutions of the stationary quasi-1D GPE allows us to determine, in the quasi-1D limit, the regimes of low γ in which highly soliton-like ground states can be realized (Section III D). We then consider the 3D GPE in Section IV. The system then has a second free parameter in addition to γ ; we choose this to be κ , the (dimensionless) trap anisotropy, which is defined in Section IV A. In Sections IV B to IV E we define 3D Gaussian and soliton ansatzes, adapted from their quasi-1D analogs and each parametrized by an axial and a radial length, and find the energy-minimizing lengths for each ansatz. In general this requires only a very simple numerical procedure, and in the limit of a waveguide-like trap can be expressed analytically (Section IV F). In Section IV G we compare the ansatz solutions to highly accurate numerical solutions of the stationary 3D GPE and, in Section IV H assess the potential for realizing truly soliton-like ground states. Finally, Section V comprises the conclusions.

II. SYSTEM OVERVIEW

We consider a BEC of N atoms of mass m and (attractive) s -wave scattering length $a_s < 0$, held within a cylindrically symmetric, prolate (the radial frequency ω_r is greater than the axial frequency ω_x) harmonic trap. The ground state is described by the stationary Gross-Pitaevskii equation

$$\left[-\frac{\hbar^2}{2m} \nabla^2 + V(\mathbf{r}) - \frac{4\pi N |a_s| \hbar^2}{m} |\psi(\mathbf{r})|^2 - \lambda \right] \psi(\mathbf{r}) = 0, \quad (1)$$

where the trapping potential $V(\mathbf{r}) = m[\omega_x^2 x^2/2 + \omega_r^2(y^2 + z^2)/2]$, λ is a real eigenvalue, and the Gross-Pitaevskii wavefunction $\psi(\mathbf{r})$ is normalized to one. This equation is generated by the classical field Hamiltonian (through the functional derivative $\delta H[\psi]/\delta \psi^* = \lambda \psi$)

$$H[\psi] = \int d\mathbf{r} \left[\frac{\hbar^2}{2m} |\nabla \psi(\mathbf{r})|^2 + V(\mathbf{r}) |\psi(\mathbf{r})|^2 - \frac{2\pi N |a_s| \hbar^2}{m} |\psi(\mathbf{r})|^4 \right]. \quad (2)$$

This functional of the classical field ψ describes the total energy per particle, and the ground state solution minimizes the value of this functional.

When dealing with variational ansatzes for the ground state solution, we proceed by analytically minimizing an energy functional in the same form as Eq. (2) for a given ansatz. In contrast, highly accurate numerical ground states are more conveniently obtained by solving a stationary GPE of the same form as Eq. (1).

III. QUASI-1D LIMIT

A. Reduction to 1D and rescaling

For sufficiently tight radial confinement ($\omega_r \gg \omega_x$), such that the atom-atom interactions are nonetheless essentially 3D [$a_s \ll (\hbar/m\omega_r)^{1/2}$] it is conventional [10–15] to assume a reduction to a quasi-1D stationary GPE

$$\left[-\frac{\hbar^2}{2m} \frac{\partial^2}{\partial x^2} + \frac{m\omega_x^2 x^2}{2} - g_{1D} N |\psi(x)|^2 - \lambda \right] \psi(x) = 0. \quad (3)$$

Typically $\psi(\mathbf{r})$ is taken to be factorized into $\psi(x)$ and the radial harmonic ground state $(m\omega_r/\pi\hbar)^{1/2} \exp(-m\omega_r[y^2 + z^2]/2\hbar)$, such that $g_{1D} = 2\hbar\omega_r|a_s|$. In the absence of the axial harmonic confining potential ($\omega_x \rightarrow 0$), there exist exact bright soliton solutions to this equation of the general form¹

$$\frac{1}{2b_x^{1/2}} \text{sech}\left(\frac{[x - vt + C]}{2b_x}\right) e^{iv(x-vt)m/\hbar} e^{img_{1D}^2 N^2 t/8\hbar^3} e^{imv^2 t/2\hbar} e^{iD}, \quad (4)$$

¹ Equation (4) describes solutions of unit norm. More general soliton solutions $(B/2b_x^{1/2}) \text{sech}(B[x - vt + C]/2b_x) e^{iv(x-vt)m/\hbar} e^{iB^2 mg_{1D}^2 N^2 t/8\hbar^3} e^{imv^2 t/2\hbar} e^{iD}$ have norm B (and effective mass $\eta = B/4$), as arise when considering several solitons simultaneously.

where $b_x \equiv \hbar^2/mg_{1D}N$ is a length scale characterizing the soliton's spatial extent, v is the soliton velocity, C is an arbitrary displacement, and D is an arbitrary phase.

This effective 1D Gross-Pitaevskii equation contains two key length scales: the axial harmonic length $a_x \equiv (\hbar/m\omega_x)^{1/2}$, and the soliton length b_x . A mathematically convenient way to express the single free parameter of Eq. (3) is as the square of the ratio of these two length scales;

$$\gamma \equiv \left(\frac{b_x}{a_x}\right)^2 \equiv \frac{\hbar\omega_x}{4m\omega_r^2|a_s|^2N^2}. \quad (5)$$

This parametrization is achieved by working in “soliton units”; lengths are expressed in units of b_x and energies are expressed in units of $mg_{1D}N^2/\hbar^2$. This system can be codified as $\hbar = m = g_{1D}N = 1$, and yields the dimensionless quasi-1D GPE

$$\left[-\frac{1}{2}\frac{\partial^2}{\partial x^2} + \frac{\gamma^2 x^2}{2} - |\psi(x)|^2 - \lambda\right]\psi(x) = 0, \quad (6)$$

in which γ can be interpreted as a dimensionless trap frequency [15]. The corresponding classical field Hamiltonian is

$$H_{1D}[\psi] = \int dx \left[\frac{1}{2} \left| \frac{\partial}{\partial x} \psi(x) \right|^2 + \frac{\gamma^2 x^2}{2} |\psi(x)|^2 - \frac{1}{2} |\psi(x)|^4 \right]. \quad (7)$$

The choice of γ for the single free parameter in the 1D GPE [Eq. (6)] and the classical field Hamiltonian [Eq. (7)] can be most directly pictured as choosing to hold interaction strength constant while varying the axial trap strength, parametrized by γ . Experimentally, however, any of ω_x , ω_r , a_s , and N may be varied in order to vary γ . In the case $\gamma = 0$ the exact ground state solution is a single, stationary bright soliton: $\psi(x) = \text{sech}(x/2)/2$. In the following subsections we develop analytic variational solutions $\psi(x)$ for general γ . Comparing these solutions to highly accurate numerical solutions of the quasi-1D GPE then gives a picture of the behavior of the ground state with γ . Furthermore, these quasi-1D variational solutions motivate the later 3D variational solutions and yield several mathematical expressions which reappear in the more complex 3D calculations.

B. Variational solution: Gaussian ansatz

We first consider the Gaussian variational ansatz

$$\psi(x) = \left(\frac{\gamma}{\pi\ell_G^2}\right)^{1/4} e^{-\gamma x^2/2\ell_G^2}, \quad (8)$$

where the variational parameter, ℓ_G , quantifies the axial length. In the trap-dominated limit ($\gamma \rightarrow \infty$), the true solution tends to a Gaussian with $\ell_G = 1$. Substituting Eq. (8) into Eq. (7) yields (using identities from Appendix A)

$$H_{1D}(\ell_G) = \frac{\gamma}{4} \left(\ell_G^2 + \frac{1}{\ell_G^2} - \frac{2}{(2\pi\gamma)^{1/2}\ell_G} \right), \quad (9)$$

where H_{1D} is now expressed as a function of the axial length ℓ_G . Setting $\partial H_{1D}/\partial \ell_G = 0$ reveals that the variational energy described by Eq. (9) is minimized when ℓ_G is a positive, real solution to the quartic equation

$$\ell_G^4 + \frac{\ell_G}{(2\pi\gamma)^{1/2}} - 1 = 0. \quad (10)$$

The positive, real solution to this quartic is (see solution in Appendix B)

$$\ell_G = \frac{[\chi(\gamma)]^{1/2}}{2^{4/3}(\pi\gamma)^{1/6}} \left\{ \left[\left(\frac{2}{\chi(\gamma)} \right)^{3/2} - 1 \right]^{1/2} - 1 \right\}, \quad (11)$$

where we have, for notational convenience, defined χ to have γ -dependence such that

$$\chi(\gamma) = \left[1 + \left(1 + \frac{1024\pi^2\gamma^2}{27} \right)^{1/2} \right]^{1/3} + \left[1 - \left(1 + \frac{1024\pi^2\gamma^2}{27} \right)^{1/2} \right]^{1/3}. \quad (12)$$

C. Variational solution: soliton ansatz

Secondly, we consider a soliton ansatz

$$\psi(x) = \frac{1}{2\ell_S^{1/2}} \text{sech}\left(\frac{x}{2\ell_S}\right), \quad (13)$$

where the variational parameter, ℓ_S , again quantifies the axial length. In the axially un-trapped limit ($\gamma \rightarrow 0$), the true solution tends to a classical bright soliton, as described by the above ansatz with $\ell_S = 1$. The variational energy per particle is given by (using identities from Appendix A)

$$H_{1D}(\ell_S) = \frac{\pi^2\gamma^2}{6} \left(\ell_S^2 + \frac{1}{4\pi^2\gamma^2\ell_S^2} - \frac{1}{2\pi^2\gamma^2\ell_S} \right), \quad (14)$$

which is minimized when

$$\ell_S^4 + \frac{\ell_S}{4\pi^2\gamma^2} - \frac{1}{4\pi^2\gamma^2} = 0. \quad (15)$$

Again, this quartic can be solved analytically (see solution in Appendix B) to give the positive, real minimizing value of ℓ_S ;

$$\ell_S = \frac{[\chi(\gamma)]^{1/2}}{2^{11/6}(\pi\gamma)^{2/3}} \left\{ \left[\left(\frac{2}{\chi(\gamma)} \right)^{3/2} - 1 \right]^{1/2} - 1 \right\}, \quad (16)$$

with χ defined as in Eq. (12).

D. Analysis and comparison to 1D numerical solutions

The energy-minimizing axial lengths ℓ_G and ℓ_S , defined by Eq. (11) and Eq. (16) respectively, are shown as a function of

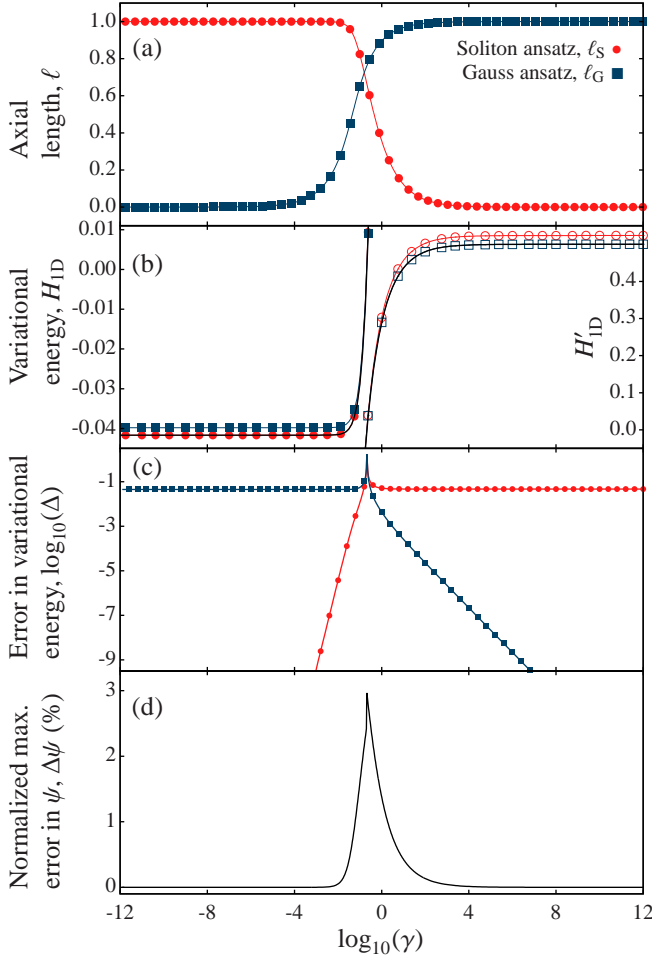


FIG. 1. Comparison of quasi-1D variational and numerical solutions: (a) Energy-minimizing axial lengths ℓ_G (Gaussian ansatz, squares) and ℓ_S (soliton ansatz, circles) for the quasi-1D GPE. (b) Minimum variational energy compared with the numerically calculated ground state energy E_{1D} (black line) for each ansatz: for low γ we show H_{1D} (solid symbols), which tends to $-1/24$ as $\gamma \rightarrow 0$; for high γ we show $H'_{1D} = H_{1D}/\gamma$ (hollow symbols), which tends to $1/2$ as $\gamma \rightarrow \infty$ (H'_{1D} is equal to the energy expressed in the “harmonic units,” $\hbar = m = \omega_x = 1$). (c) Relative error in the variational energy, $\Delta = (H_{1D} - E_{1D})/E_{1D}$. (d) Normalized maximum deformation of the best-fitting ansatz wavefunction ψ_{Ansatz} with respect to the numerical ground state ψ_0 , $\Delta\psi = \max(|\psi_{\text{Ansatz}} - \psi_0|)/\max(\psi_0)$, expressed as a percentage. For clarity in (a,b) [(c)], every 16th [20th] datum is marked by a symbol.

γ in Fig. 1(a). There is no collapse instability in the quasi-1D GPE, and solutions are obtained for all (positive, real) γ . As intended by the chosen forms of the ansatzes, the limiting cases are $\ell_G \rightarrow 1$ as $\gamma \rightarrow \infty$ and $\ell_S \rightarrow 1$ as $\gamma \rightarrow 0$. To evaluate the accuracy of the ansatzes for general γ , we compare each ansatz with the numerically determined ground state of the quasi-1D GPE. The computation of a numerically exact ground state $\psi_0(x)$, and the corresponding ground state energy E_{1D} , uses a pseudospectral method in a basis of symmetric Gauss-Hermite functions; this is a simplified version of the pseudospectral method used for 3D calculations, which

is explained in more detail in the next section. Several quantities are compared in Fig. 1(b–d): the variational minimum energies H_{1D} for each ansatz and the numerical ground state energy E_{1D} are shown in Fig. 1(b); the relative error between H_{1D} and E_{1D} , defined as $\Delta = (H_{1D} - E_{1D})/|E_{1D}|$, is shown for each ansatz in Fig. 1(c); and the maximum difference between the most appropriate ansatz wavefunction (that with lowest Δ) and the numerical ground state wavefunction, expressed as a percentage of the maximum value of the numerically exact ground state, $\Delta\psi = \max(|\psi_{\text{Ansatz}} - \psi_0|)/\max(\psi_0)$ [Fig. 1(d)]. All the shown computed quantities are insensitive to a doubling of the numerical basis size from 500 to 1000 states.

Both the Gaussian and soliton ansatzes provide an excellent approximation to the exact solutions over a large range of γ . In the regimes where the relative error in the energy Δ becomes significantly lower than 10^{-9} in particular, the difference between the ansatz solutions and numerical solutions becomes generally indistinguishable from numerical round-off error. For the Gaussian ansatz the convergence to this regime is noticeably slower than for the soliton ansatz [Fig. 1(c)]. This effect is a consequence of the parametrization in terms of γ and the corresponding “soliton units”: increasing γ leads not only to higher trap strength, but also to higher peak densities $|\psi(x)|^2$, and hence a stronger nonlinear effect.

For later comparison to the 3D case, it is useful to define a benchmark value of the relative error Δ that indicates excellent agreement between the ansatz and the numerically exact solution. Such a definition, however, will vary according to purpose. As our objectives in this paper relate significantly to the *shape* of the ground state, this forms the basis of our benchmark; a maximum deformation of the wavefunction below 0.1% of the peak value [as measured by $\Delta\psi$ in Fig. 1(d)] corresponds very closely to $\Delta < 10^{-5}$. Because the relative error Δ saturates to a background value of $\approx 10^{-1}$ in regimes where the chosen ansatz is inapplicable, a value of Δ four orders of magnitude below this background value thus corresponds to an excellent match in shape between the ansatz and the numerically exact solution. With respect to this benchmark, the Gaussian ansatz represents an excellent fit for $\log_{10}(\gamma) > 1.15$, while the ground state is highly soliton-like (the soliton ansatz represents an excellent fit) for $\log_{10}(\gamma) < -0.95$.

IV. BRIGHT SOLITARY WAVE GROUND STATES IN 3D

A. Rescaling to effective 1D soliton units

We now consider the cylindrically symmetric 3D Gross-Pitaevskii equation [Eq. (1)]. Compared to the quasi-1D effective Gross-Pitaevskii equation [Eq. (6)], three-dimensionality introduces an additional relevant length scale, the radial harmonic length $a_r = (\hbar/m\omega_r)^{1/2}$. We incorporate this into the dimensionless trap anisotropy $\kappa \equiv \omega_r/\omega_x$, which forms an additional free parameter. Expressed in the same “soliton units” as Eq. (6), Eq. (1) becomes

$$\left[-\frac{1}{2}\nabla^2 + V(\mathbf{r}) - \frac{2\pi}{\kappa\gamma}|\psi(\mathbf{r})|^2 - \lambda \right] \psi(\mathbf{r}) = 0, \quad (17)$$

with corresponding energy functional

$$H_{3D}[\psi] = \int d\mathbf{r} \left[\frac{1}{2} \nabla \psi(\mathbf{r}) \cdot \nabla \psi^*(\mathbf{r}) + V(\mathbf{r})|\psi(\mathbf{r})|^2 - \frac{\pi}{\kappa\gamma} |\psi(\mathbf{r})|^4 \right], \quad (18)$$

where $V(\mathbf{r}) = \gamma^2[x^2 + \kappa^2(y^2 + z^2)]/2$.

In the following subsections we obtain variational solutions for general κ and γ using ansatzes similar to the Gaussian and soliton ansatzes employed in the previous section, with an additional variable-width Gaussian radial profile. Contrary to the case in the quasi-1D limit, a self-consistent energy-minimizing solution for both the axial and radial length parameters cannot be expressed entirely analytically. However, we reduce the numerical work required to the simultaneous solution of two equations, and introduce a straightforward iterative technique to achieve this. We also consider the case of a waveguide-like trap ($\omega_x = 0$) separately, where an entirely analytic variational solution exists (Section IV F). Subsequently, in Section IV G, we again compare the ansatz solutions to high-accuracy numerics.

B. Variational solution: Gaussian ansatz

We first consider an ansatz composed of Gaussian axial and radial profiles. We phrase this as

$$\psi(\mathbf{r}) = \frac{\kappa^{1/2} \gamma^{3/4} k_G}{\pi^{3/4} \ell_G^{1/2}} e^{-\kappa \gamma k_G^2 (y^2 + z^2)/2} e^{-\gamma x^2 / 2 \ell_G^2}. \quad (19)$$

Here, the first variational parameter, ℓ_G , quantifies the axial length of the ansatz in analogy to the quasi-1D case. The *reciprocal* of the second variational parameter, k_G^{-1} , quantifies the radial length of the ansatz. In the trap-dominated limit ($\gamma \rightarrow \infty$) both these lengths approach unity ($\{\ell_G, k_G\} \rightarrow 1$). Substitution of this ansatz into Eq. (18) yields (using identities from Appendix A)

$$H_{3D}(\ell_G, k_G) = \frac{\gamma}{4} \left(\ell_G^2 + \frac{1}{\ell_G^2} - \frac{2k_G^2}{(2\pi\gamma)^{1/2} \ell_G} + 2\kappa k_G^2 + \frac{2\kappa}{k_G^2} \right) \quad (20)$$

Setting the partial derivatives with respect to both ℓ_G and k_G equal to zero, we deduce that ℓ_G must solve the quartic equation

$$\ell_G^4 + \frac{k_G^2 \ell_G}{(2\pi\gamma)^{1/2}} - 1 = 0, \quad (21)$$

and that k_G must solve

$$k_G = \left(\frac{(2\pi\gamma)^{1/2} \kappa \ell_G}{(2\pi\gamma)^{1/2} \kappa \ell_G - 1} \right)^{1/4}. \quad (22)$$

From Eq. (22) it follows that we must have $\ell_G > 1/(2\pi\gamma)^{1/2} \kappa$ to obtain a physically reasonable solution, i.e., a real, positive value of k_G , consistent with our initial ansatz.

For a given such value of k_G , Eq. (21) is solved (see solution in Appendix B) by

$$\ell_G = \frac{[\chi(\gamma k_G^{-4})]^{1/2} k_G^{2/3}}{2^{4/3} (\pi\gamma)^{1/6}} \left\{ \left[\left(\frac{2}{\chi(\gamma k_G^{-4})} \right)^{3/2} - 1 \right]^{1/2} - 1 \right\}, \quad (23)$$

with χ defined as in Eq. (12).

C. Analysis of Gaussian ansatz solution

Contrary to the quasi-1D limit, minimization of the variational energy in 3D requires simultaneous solution of two equations for the radial length, k_G^{-1} , and the axial length, ℓ_G . These equations are, respectively, Eq. (22) and [rearranged from Eq. (21)]

$$k_G = \left[\frac{(2\pi\gamma)^{1/2}}{\ell_G} (1 - \ell_G^4) \right]^{1/2}. \quad (24)$$

These equations dictate that physical solutions must have

$$\frac{1}{(2\pi\gamma)^{1/2} \kappa} < \ell_G < 1, \quad (25)$$

and hence that $\gamma > 1/2\pi\kappa^2$ must be satisfied in order for physical solutions to exist.

Where solutions exist, they must be found numerically. However, a very practical method of numerical solution follows from the shape of the ℓ_G surface defined by Eq. (23), and shown in Fig. 2(a), which is a decreasing function of k_G for all (real, positive) γ . The method can be considered graphically, in terms of locating the intersection(s) of Eq. (22) and Eq. (24). These curves are shown, for various κ , in Fig. 2(b–d), along with the lower bound from inequality (25). Below a κ -dependent threshold value of γ the curves fail to intersect, indicating instability of the BEC to collapse. At the threshold value [dotted curves in Fig. 2(b–d)] there is exactly one intersection, and above the threshold value [other curves in Fig. 2(b–d)] there are two intersections. In the latter case the higher- ℓ_G intersection, which smoothly deforms to the limiting case $\{\ell_G, k_G\} \rightarrow 1$ as $\gamma \rightarrow \infty$, represents the physical, minimal-energy variational solution. This solution can be located using a simple “staircase” method: substituting a trial value \bar{k}_G , satisfying $1 \leq \bar{k}_G < k_G$, into Eq. 23 produces a trial value, $\bar{\ell}_G$, satisfying $\ell_G < \bar{\ell}_G \leq 1$, and subsequently substituting this trial value into Eq. 22 produces an iterated trial value, \bar{k}'_G , satisfying $\bar{k}_G < \bar{k}'_G < k_G$. Thus, beginning with $\bar{k}_G = 1$, iteration of this process converges the trial values to the true k_G and ℓ_G .

The physical solutions to equations (21) and (22) for different anisotropies κ are shown on the ℓ_G surface, and projected into the ℓ_G - γ plane, in Fig. 2(a). These solutions are also shown as black crosses in the ℓ_G - k_G plane in Figs. 2(b–d), where they form a line connecting the physical-solution intersections of Eq. (22) and Eq. (24) for the various γ shown. In Fig. 2(a) the collapse instability is manifest as a rapid rise in k_G — corresponding to a decrease in radial extent — and

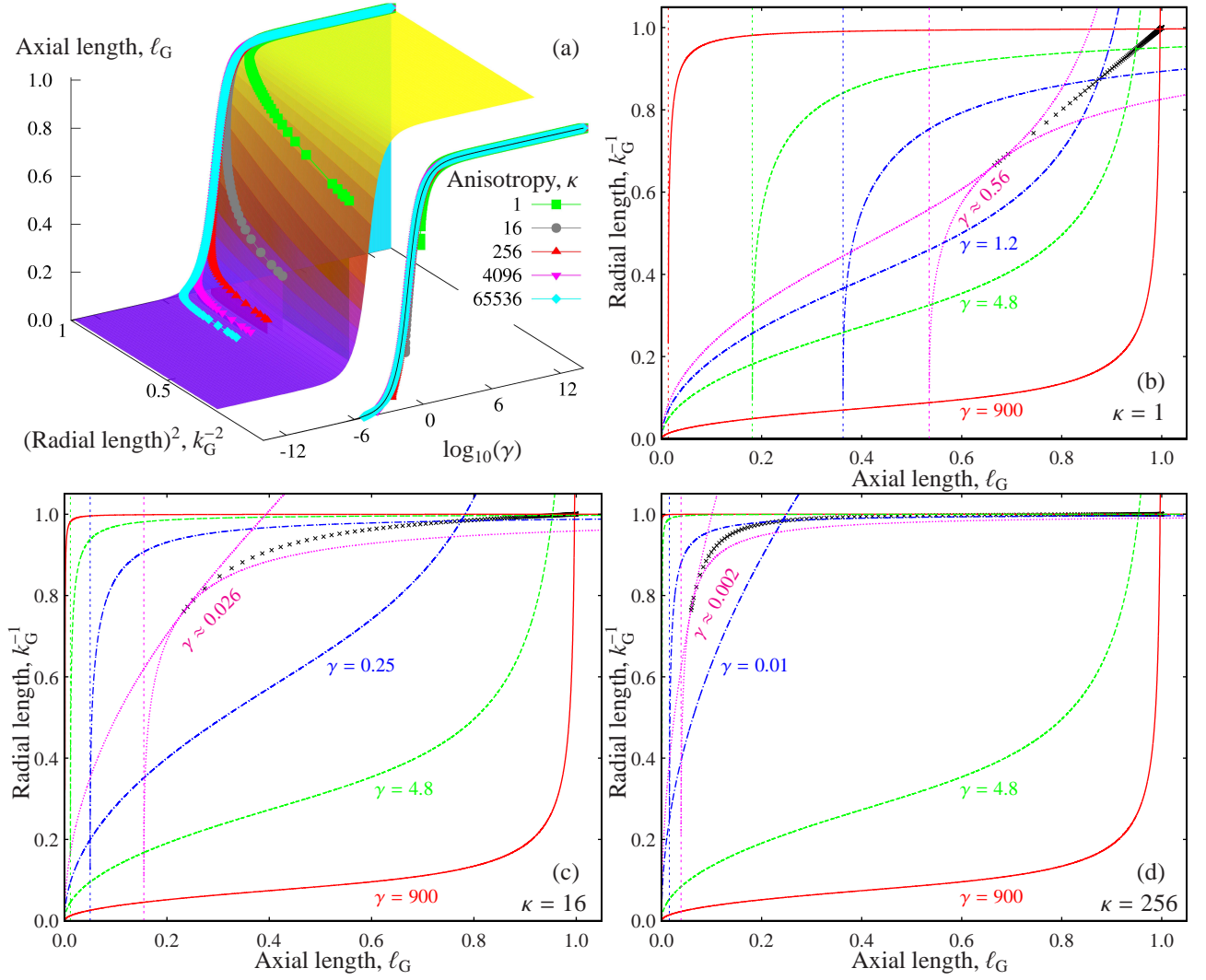


FIG. 2. Energy-minimizing variational parameters for the 3D GPE using a Gaussian ansatz: (a) axial length ℓ_G as a function of the radial length k_G^{-1} and the parameter γ [Eq. 23]. Lines show the simultaneous solutions of equations (22) and (24) for the axial length ℓ_G and radial length k_G^{-1} , for different anisotropies κ and values of γ . Projections of these solutions on the γ - ℓ_G plane are also shown; here the black line indicates the quasi-1D result [from figure 1(a)]. (b–d) Illustration of the intersections of equations (22) [lines with vertical asymptote $\ell_G = 1/(2\pi\gamma)^{1/2}\kappa$ shown with fine dashes] and (24) for various κ : the higher- ℓ_G intersection, which corresponds to a physical solution for the axial length ℓ_G and radial length k_G^{-1} , can be found using a “staircase” method starting from $k_G = 1$. The numerical solutions obtained this way, and shown by points in (a), are shown by crosses in (b–d). The lowest values of γ plotted in (b–d) are the lowest for which a self-consistent Gaussian ansatz solution is found.

fall in ℓ_G — corresponding to a decrease in axial extent — just above a κ -dependent threshold value of γ . There are no self-consistent solutions for these quantities below this collapse threshold. For increasing anisotropies κ , this collapse threshold occurs at lower values of γ . For the highest two values of κ considered the collapse threshold lies in the regime where ℓ_G is already approaching 0; our analysis of the Gaussian ansatz in the quasi-1D limit indicates that the 3D Gaussian ansatz will be a poor approximation to the true solution in this regime. Importantly, for γ above the collapse threshold the projected curves for each anisotropy agree well with the Gaussian ansatz in the quasi-1D GPE, suggesting that the Gaussian ansatz gives a good approximation to the true solu-

tion here.

D. Variational solution: soliton ansatz

Secondly, we consider a soliton ansatz composed of a axial sech profile and a radial Gaussian profile. We phrase this as

$$\psi(\mathbf{r}) = \frac{\gamma^{1/2}\kappa^{1/2}k_S}{(2\pi\ell_S)^{1/2}} e^{-\kappa\gamma k_S^2(y^2+z^2)/2} \text{sech}(x/2\ell_S). \quad (26)$$

As with the 3D Gaussian ansatz, the first variational parameter, ℓ_G , quantifies the axial length of the ansatz and the *reciprocal* of the second variational parameter, k_G^{-1} , quantifies its

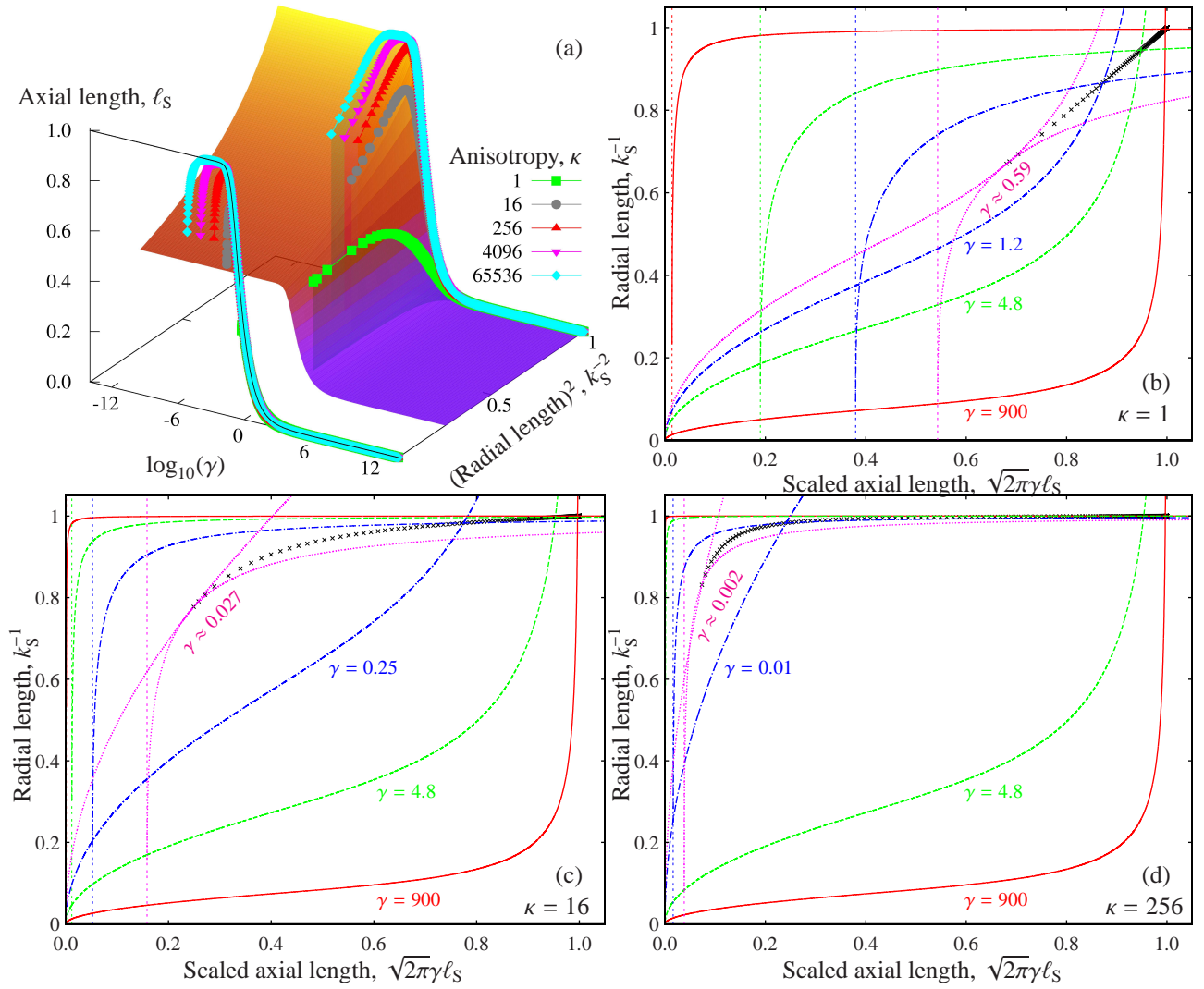


FIG. 3. Energy-minimizing variational parameters for the 3D GPE using a soliton ansatz: (a) axial length ℓ_S as a function of the radial length k_S^{-1} and the parameter γ [Eq. 30]. Lines show the simultaneous solutions of equations (33) and (34) for the axial length ℓ_S and radial length k_S^{-1} , for different anisotropies κ and values of γ . Projections of these solutions on the γ - ℓ_S plane are also shown; here the black line indicates the quasi-1D result [from figure 1(a)]. (b–d) Illustration of the intersections of equations (33) [lines with vertical asymptote $\ell_S = (\pi/3)/(2\pi\gamma)^{1/2}\kappa$ shown with fine dashes] and (34) for various κ : the higher- ℓ_S intersection, which corresponds to a physical solution for the axial length ℓ_S and radial length k_S^{-1} , can be found using a “staircase” method starting from $k_S = 1$. The numerical solutions obtained this way, and shown by points in (a), are shown by crosses in (b–d). The lowest values of γ plotted in (b–d) are the lowest for which a self-consistent soliton ansatz solution is found.

radial length. In the quasi-1D limit both lengths consequently approach unity ($\{\ell_G, k_G\} \rightarrow 1$). Substituting this ansatz into Eq. (18) yields (using identities from Appendix A)

$$H_{3D}(\ell_S, k_S) = \frac{\pi^2 \gamma^2}{6} \left(\ell_S^2 + \frac{1}{4\pi^2 \gamma^2 \ell_S^2} - \frac{k_S^2}{2\pi^2 \gamma^2 \ell_S} + \frac{3\kappa k_S^2}{\pi^2 \gamma} + \frac{3\kappa}{\pi^2 \gamma k_S^2} \right). \quad (27)$$

Once again, setting partial derivatives with respect to both ℓ_S and k_S equal to zero allows us to deduce that:

$$\ell_S^4 + \frac{k_S^2 \ell_S}{4\pi^2 \gamma^2} - \frac{1}{4\pi^2 \gamma^2} = 0, \quad (28)$$

and that k_S must solve

$$k_S = \left(\frac{6\kappa \gamma \ell_S}{6\kappa \gamma \ell_S - 1} \right)^{1/4}. \quad (29)$$

From Eq. (29) it follows that we must have $\ell_S > 1/6\kappa\gamma$ to obtain a physically reasonable solution, i.e., a real, positive value of k_S , consistent with our initial ansatz. For a given such

value of k_S , Eq. (28) is solved (see solution in Appendix B) by

$$\ell_S = \frac{[\chi(\gamma k_S^{-4})]^{1/2} k_S^{2/3}}{2^{11/6}(\pi\gamma)^{2/3}} \left\{ \left[\left(\frac{2}{\chi(\gamma k_S^{-4})} \right)^{3/2} - 1 \right]^{1/2} - 1 \right\}, \quad (30)$$

with χ defined as in Eq. (12).

E. Analysis of soliton ansatz solution

As in the case of the Gaussian ansatz, minimization of the variational energy in 3D requires the simultaneous solution of equations for the radial length k_S^{-1} and the axial length ℓ_S . These equations are, respectively, Eq. (29) and [rearranged from Eq. (28)]

$$k_S = \left[\frac{1}{\ell_S} \left(1 - 4\pi^2 \gamma^2 \ell_S^4 \right) \right]^{1/2} \quad (31)$$

These equations dictate that physical solutions must have

$$\frac{1}{6\kappa\gamma} < \ell_S < \frac{1}{(2\pi\gamma)^{1/2}} \quad (32)$$

and hence that $\gamma > (\pi/3)^2/2\pi\kappa^2$ must be satisfied in order for physical solutions to exist. These equations and constraints can be further simplified by casting them in terms of $\ell'_S = (2\pi\gamma)^{1/2}\ell_S$; this yields two equations,

$$k_S = \left(\frac{(2\pi\gamma)^{1/2}\kappa\ell'_S}{(2\pi\gamma)^{1/2}\kappa\ell'_S - \pi/3} \right)^{1/4} \quad (33)$$

and

$$k_S = \left[\frac{(2\pi\gamma)^{1/2}}{\ell'_S} \left(1 - \ell'^4_S \right) \right]^{1/2}, \quad (34)$$

and an inequality,

$$\frac{\pi/3}{(2\pi\gamma)^{1/2}\kappa} < \ell'_S < 1, \quad (35)$$

which are extremely similar to those encountered in the case of the Gaussian ansatz. The numerical solution of these equations for the physical solution, which can only exist when $\gamma > (\pi/3)^2/2\pi\kappa^2$, follows the same procedure as used for the Gaussian ansatz.

Variational-energy-minimizing solutions to the soliton ansatz equations for different anisotropies κ are shown in Fig. 3; these are shown superimposed on the ℓ_S surface and projected into the ℓ_S - γ plane in Fig. 3(a), and alongside equations (28) and (29) and inequality (35) in Fig. 3(b-d). The collapse instability is even more evident in the soliton ansatz than in the Gaussian ansatz, since it occurs in a region with a larger background value of ℓ_S . Once again, the collapse is manifest as a rapid rise in k_S and drop in ℓ_S — corresponding to both axial and radial contraction of the solution — immediately prior to a κ -dependent threshold value of γ . Below the threshold, no

self-consistent solutions exist. For increasing anisotropies κ , this collapse threshold again occurs at lower values of γ . In contrast to the case of the Gaussian ansatz, however, the collapse instability precludes solutions in exactly the limit where one expects the soliton ansatz to be accurate ($\gamma \rightarrow 0$). This property of the collapse instability severely restricts the possibility of observing highly bright-soliton-like ground states in 3D. The solution curves in Fig. 3(a) illustrate that this effect is worst for low trap anisotropies κ , but is to some extent mitigated for higher κ . However, a full comparison with numerically exact solutions is necessary to quantify these effects; we undertake such a comparison in Section IV G.

F. Variational solution: waveguide configuration

In broad experimental terms, the collapse instability sets a maximum value for the ratio of interaction strength to trap strength (equivalent to a minimum value of γ) which increases (and hence the minimum value of γ decreases) with the trap anisotropy κ . In the context of atomic BEC experiments one would typically think of controlling the interaction-trap strength ratio by varying either $|a_s|$ or N while holding ω_r and ω_x constant; in this situation the collapse instability places a trap-anisotropy-dependent upper limit on the product $|a_s|N$. However, the minimum value of γ does not increase without limit in the trap anisotropy κ : In an experiment one can, in principle, remove all axial trapping to create a waveguide-like configuration; in this case $\omega_x = 0$ and the trap anisotropy $\kappa \rightarrow \infty$, while the parameter $\gamma \rightarrow 0$. In this limit a reparametrization is necessary, and only needs to be performed for the soliton ansatz, which is clearly more appropriate in this context.

Elimination of the axial trap eliminates one of the two free parameters of the 3D GPE [Eq. (17)]. The remaining free parameter is $\Gamma = \gamma\kappa = (a_r/2|a_s|N)^2$, where $a_r = (\hbar/m\omega_r)^{1/2}$ is the radial harmonic oscillator length scale. The soliton ansatz may be re-written in terms of Γ as

$$\psi(\mathbf{r}) = \frac{\Gamma^{1/2}k_S}{(2\pi\ell_S)^{1/2}} e^{-\Gamma k_S^2(y^2+z^2)/2} \text{sech}(x/2\ell_S). \quad (36)$$

Substituting this into Eq. (18) with $\omega_x = 0$ yields (using identities from Appendix A),

$$H_{3D}(\ell_S, k_S) = \left(\frac{1}{24\ell_S^2} - \frac{k_S^2}{12\ell_S} + \frac{\Gamma k_S^2}{2} + \frac{\Gamma}{2k_S^2} \right), \quad (37)$$

from which we deduce that the energy-minimizing variational parameters satisfy

$$\ell_S = \frac{1}{k_S^2} \quad (38)$$

and

$$k_S = \left(\frac{6\Gamma\ell_S}{6\Gamma\ell_S - 1} \right)^{1/4}. \quad (39)$$

Contrary to the more general 3D case, an analytic simultaneous solution of Eq. (38) and Eq. (39) exists when ℓ_S satisfies

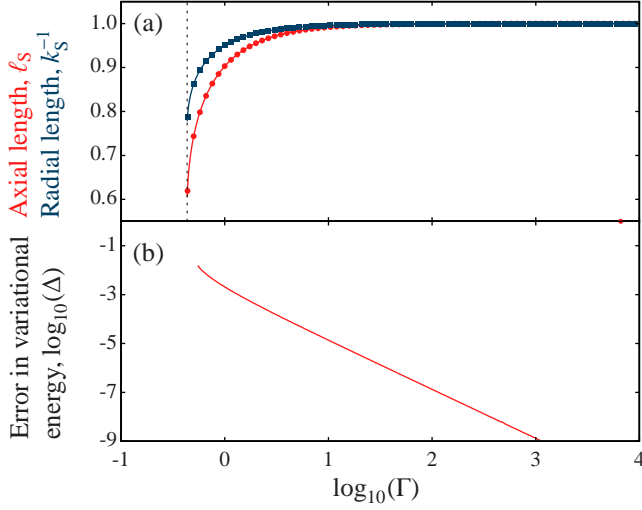


FIG. 4. Comparison of 3D variational and numerical solutions in a waveguide configuration ($\omega_x = 0$): (a) Energy-minimizing axial length ℓ_S and radial length k_S^{-1} for the soliton ansatz. Solutions, given by Eq. (41), exist for all $\Gamma = \kappa\gamma > 3^{1/2}/4$. (b) Relative error in the minimum variational energy of the soliton ansatz, $\Delta = (H_{3D} - E_{3D})/E_{3D}$, where E_{3D} is the numerically determined ground state energy.

the depressed cubic equation

$$\ell_S^3 - \ell_S + \frac{1}{6\Gamma} = 0. \quad (40)$$

Using the general solution for a depressed cubic equation from Appendix B, one finds that the physical root (with real, positive ℓ_S satisfying the limit $\ell_S \rightarrow 1$ as $\Gamma \rightarrow \infty$) is given by

$$\ell_S = \left[-\frac{1}{12\Gamma} + \frac{1}{3^{3/2}\Gamma} \left(\frac{3}{16} - \Gamma^2 \right)^{1/2} \right]^{1/3} + \left[-\frac{1}{12\Gamma} - \frac{1}{3^{3/2}\Gamma} \left(\frac{3}{16} - \Gamma^2 \right)^{1/2} \right]^{1/3}. \quad (41)$$

Consequently, solutions only exist for $\Gamma > 3^{1/2}/4$, as shown in Fig. 4(a).

G. Comparison to 3D numerical solutions

The variational energy-minimizing axial lengths ℓ_G and ℓ_S are shown as functions of γ in Fig. 5(a) for the general 3D case; for the waveguide limit both axial and radial lengths ℓ_S and k_S^{-1} are shown as functions of Γ in Fig. 4(a). As in the quasi-1D case, we quantitatively evaluate the accuracy of the ansatz solutions for general γ (Γ) by comparing the variational minimum energy H_{3D} with the numerically determined ground state energy E_{3D} . We calculate E_{3D} using a pseudospectral method in a basis of optimally-scaled harmonic oscillator eigenstates; this is formed from a tensor product of symmetric Gauss-Hermite functions (axial direction) and generalized Laguerre functions (radial direction). The ansatz

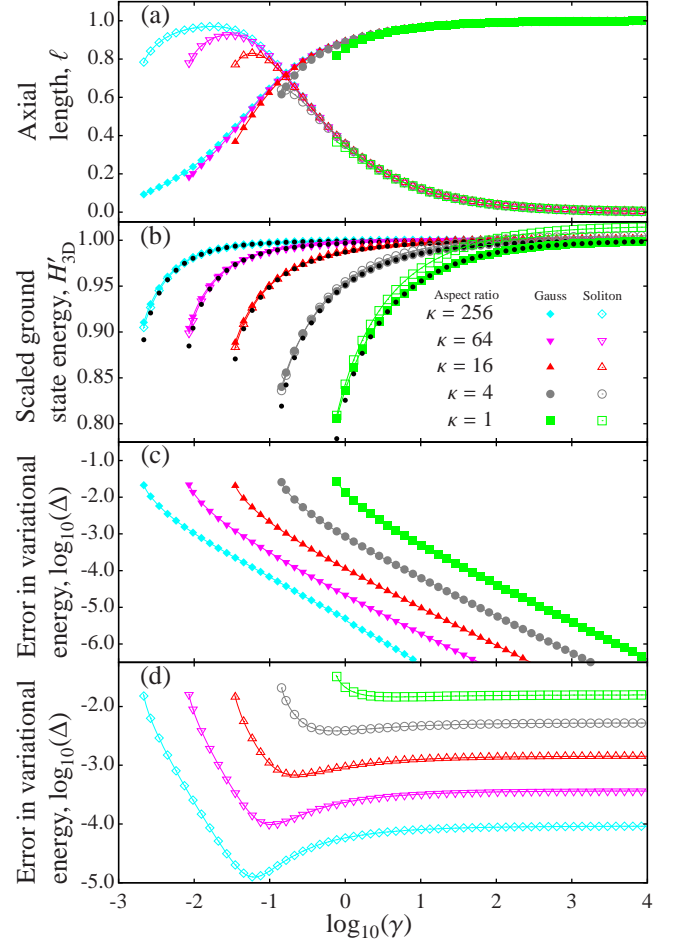


FIG. 5. Comparison of 3D variational and numerical solutions: (a) Energy-minimizing axial lengths ℓ_G (Gaussian ansatz, solid symbols) and ℓ_S (soliton ansatz, hollow symbols). (b) Scaled variational energies $H'_{3D} = \kappa H_{3D}/\gamma(\kappa + 1/2)$ (a similarly scaled ground state energy $E'_{3D} = \kappa E_{3D}/\gamma(\kappa + 1/2)$ tends to 1 in the limit $\gamma \rightarrow \infty$ for all anisotropies κ) compared with the numerically calculated ground state energies E_{3D} (black dots). (c,d) Normalized relative error in the variational energy $\Delta = (H_{3D} - E_{3D})/E_{3D}$ for the Gaussian (c) and soliton (d) ansatzes. For clarity every 4th datum is marked by a symbol in (a-d).

with the lowest variational energy is used both to optimize the scaling of the basis functions and as an initial estimate for the solution. Expanding the stationary 3D GPE in such a basis produces a system of nonlinear equations which are solved iteratively using a modified Newton method. A similar method was used to solve a similar cylindrically symmetric, stationary 3D GPE, with repulsive interactions, in Ref. [47].

As in the quasi-1D case, we compare several quantities between the ansatz and numerical solutions. Fig. 5(b) shows the scaled energy $H'_{3D} = (H_{3D}/\gamma)/(\kappa + 1/2)$ in the general 3D case. This scaling is such that E'_{3D} — which is defined analogously to H'_{3D} with respect to E_{3D} — tends to 1 as $\gamma \rightarrow \infty$. Figs. 5(c) and (d) show the relative error in the variational minimum energy $\Delta = (H_{3D} - E_{3D})/E_{3D}$ for the Gaussian and soliton ansatzes, respectively. The same quantity Δ is shown

for the waveguide limit in Fig. 4(b). All quantities shown in Figs. 5 and 4 are computed using between 2000 and 12000 basis states (κ -dependent) and are insensitive to a doubling of the number of basis states.

In the general 3D case, a close inspection of Fig. 5(b–d) is necessary to reveal the overall relation between the ansatz solutions and the numerically obtained ground state. In the high- γ limit Fig. 5(b) shows that both the Gaussian variational energies (solid symbols) and the ground state energy E_{3D} (black dots) approach 1 as $\gamma \rightarrow \infty$, whereas the soliton ansatz energies (hollow symbols) tend to higher energies. This corresponds to the actual ground state most closely matching the Gaussian ansatz in this limit, as one would expect. Indeed, the relative error in variational energy, Δ , for the Gaussian ansatz [Fig. 5(c)] continues to drop exponentially with γ for all anisotropies κ , making it possible to find regimes of γ where the Gaussian ansatz gives an excellent approximation to the true ground state.

In the opposite, low- γ limit, collapse occurs at a κ -dependent value of γ ; this corresponds to the points in Fig. 5(a–d) where solution curves abruptly cease. Prior to collapse (at higher values of γ) the relation between the Gaussian ansatz, the soliton ansatz, and the actual ground state is highly dependent on the trap anisotropy κ [Fig. 5(b)]. In the case of a spherically symmetric trap, where the anisotropy $\kappa = 1$, the soliton ansatz variational energy is *never* closer to the true ground state energy E_{3D} than the Gaussian ansatz variational energy. A regime of soliton-like ground states consequently cannot exist at this low anisotropy; as the soliton ansatz is intrinsically asymmetric, this is to be expected. For higher anisotropies, the soliton ansatz energy is closer to E_{3D} than the Gaussian ansatz energy in a small regime prior to collapse. Exactly how soliton-like the ground state is in this regime can be quantitatively assessed using the relative error Δ . This is shown for the soliton ansatz in [Fig. 5(d)]. For each κ the “background” value of Δ in the limit $\gamma \rightarrow \infty$ is different; this effect is due to the decreasing size of the axial part of the energy with respect to the radial part for increasing γ . In the opposite, low- γ , limit Δ increases sharply close to the collapse point as the ground state wavefunction rapidly contracts. The maximum extent to which Δ decreases from its high- γ limit, *before* this increase due to collapse-related contraction at low γ , quantifies how soliton-like the ground state becomes in this regime. Even for the highest anisotropy shown, $\kappa = 256$, the regime of γ over which Δ drops below its background value is rather narrow, and the actual drop in Δ is only one order of magnitude. Compared to benchmark of Section III D, this indicates that the true ground state remains considerably deformed with respect to the soliton ansatz. The minimum error in the soliton ansatz energy does, however, improve with increasing anisotropy κ . Excellent agreement can be achieved in the waveguide limit ($\kappa \rightarrow \infty$): Fig. 4 shows that excellent agreement, with respect to the benchmark figure of Section III D, can be obtained for $\Gamma > 10^{3/2}$.

H. Discussion

A physical interpretation of the above results follows from considering two conditions that must be satisfied in order to realize a soliton-like ground state; (1) the radial profile should be “frozen” to a Gaussian, thus realizing a quasi-1D limit; and (2) interactions should dominate over the axial trapping. On first inspection these conditions seem mutually compatible, and satisfiable simply by increasing the radial trap frequency ω_r with other parameters held constant. However, condition (1) can only be satisfied if the maximum density remains low enough to avoid any deformation of the radial profile due to the collapse instability. Increasing ω_r leads to exactly such deformation, and ultimately to collapse, as it has the secondary effect of strongly increasing the density. This strong increase in density with ω_r is particular to the case of attractive interactions. Increasing ω_r in a repulsively-interacting BEC likewise acts to increase the density, but this increase is counteracted by the interactions; these act to reduce the density, and cause the BEC to expand axially. In the attractively-interacting case the response of the interactions is the opposite: increasing ω_r leads to axial *contraction* of the BEC. Consequently condition (1) is far harder to satisfy for an attractively-interacting BEC than a repulsively-interacting one. Responding to this problem simply by reducing the interaction strength (either through $|a_s|$ or N) leads to violation of condition (2). The nature of the problem is made particularly clear by considering the waveguide limit: here condition (2) is automatically satisfied ($\omega_x = 0$). This makes it possible to achieve a highly soliton-like ground state by satisfying condition (1) alone. However, such a ground state is achieved by *lowering* the product $\omega_r^{1/2}|a_s|N$, and thus by progressing towards the limit of extreme diluteness.

This physical behavior of the system presents considerable challenges for experiments aiming to realize a highly soliton-like ground state. In essence, the most desirable configuration is to have extremely high anisotropies κ , while keeping ω_r as low as possible. Realizing such a configuration through extremely low, or zero, axial trap frequencies ω_x is problematic: such frequencies are hard to set precisely experimentally as they require a very smooth potential to be generated, potentially over a considerable length. Furthermore, in the case $\omega_x = 0$ the mean-field approximation ceases to be valid for an attractively-interacting BEC; the true wavefunction should be translationally invariant in this case, but the mean-field solution breaks this symmetry [48]. Even for very low but non-zero ω_x the mean-field approximation can lose validity due to the extreme diluteness of the BEC, and the energy gap from the ground state to states with excited axial modes can become low enough to cause significant population of the excited states at experimentally feasible temperatures.

It is informative to consider the parameters used in bright solitary wave experiments to date [6–8]. None of these aimed to realize highly soliton-like ground states in the sense considered here. However, they nonetheless indicate regimes which have proved to be experimentally accessible and offer a guide to future possibilities. All have operated outside the regime of highly soliton-like ground states; direct comparison of the

experiments of Refs. [7] and [8] with our results reveals that κ is too small in these experiments ($\kappa \approx 11$ and $\kappa \approx 3$ respectively) to achieve a highly soliton-like ground state. The experiment of Ref. [6] featured an expulsive axial potential, which does not yield a value of κ suitable for direct comparison with our results. However, it is possible to assume the waveguide limit $\omega_x = 0$ in each experiment and compare the values of Γ with our results: in each case $\Gamma \lesssim 1$, outside the regime of highly soliton-like ground states. Thus, experiments with weaker traps and lower densities than previously realized with attractive condensates appear to be necessary in order to achieve a highly soliton-like ground state.

V. CONCLUSIONS

In this paper we considered attractively-interacting atomic BECs in cylindrically symmetric, prolate harmonic traps, and introduced variational ansatzes, based on Gaussian and bright-soliton profiles, for the GPE ground state. We compared new, analytic variational solutions based on these ansatzes with highly accurate numerical solutions of the GPE over an extensive parameter space, and hence determined how soliton-like the ground state is. Initially assuming the quasi-1D limit to be valid, we showed that the true solution to the GPE is (not) soliton like when interactions do (not) dominate over the trap strength. In 3D, this picture is complicated by the collapse instability; in the regime where all trap strengths dominate over the interactions a Gaussian variational ansatz gives an excellent approximation to the true, and non-soliton-like ground state. In contrast to the quasi-1D limit, however, we have shown that the regime in which the ground state is truly soliton-like (well approximated by a soliton variational ansatz) is either non-existent, or highly restricted, depending on the trap anisotropy. For low anisotropies, as one raises the strength of the interactions such that they approach and exceed the strength of the axial trap the true ground state ceases to be well-described by a Gaussian variational ansatz, but does not become well-described by a soliton variational ansatz before the interaction strength also exceeds the radial trapping strength, leading to collapse. Only by raising the anisotropy significantly can one open a parameter window in which the true ground-state becomes soliton-like before the interaction strength is sufficient to cause collapse.

Our results describe the nature of the ground state over a wide parameter regime, and offer a straightforward, accurate approximation to the full 3D GPE solution in many cases. Our results are particularly relevant for experiments using attractively-interacting condensates as they identify the potentially challenging parameter regime required to observe a truly soliton-like ground state, which would be an advantageous regime for experiments seeking to explore and exploit beyond-mean field effects such as a macroscopic superposition of bright solitons. Given that previous studies have shown that the dynamics and collisions of bright solitary waves can be soliton-like over a much wider parameter regime than our approach reveals the ground state to be, extending the variational approach used here to dynamical situations is an inter-

esting direction for future work.

ACKNOWLEDGMENTS

We thank S. L. Cornish, D. I. H. Holdaway, H. Salman and C. Weiss for discussions, and the UK EPSRC (Grant No. EP/G056781/1), the Jack Dodd Centre (S.A.G.) and Durham University (T.P.B.) for support.

Appendix A: Useful integrals

Considering a Gaussian ansatz to be proportional to $e^{-k^2 x^2}$, for completeness we reprise the following sequence of well-known integral identities, all of which are necessary to determine the corresponding variational energy functional:

$$\int_{-\infty}^{\infty} dx e^{-2k^2 x^2} = \frac{\sqrt{\pi/2}}{k} \Rightarrow \int_{-\infty}^{\infty} dx e^{-4k^2 x^2} = \frac{\sqrt{\pi}}{2k}, \quad (\text{A1})$$

$$\int_{-\infty}^{\infty} dx x^2 e^{-2k^2 x^2} = -\frac{1}{4k} \frac{\partial}{\partial k} \int_{-\infty}^{\infty} dx e^{-2k^2 x^2} = \frac{\sqrt{\pi/2}}{4k^3}, \quad (\text{A2})$$

$$\int_{-\infty}^{\infty} dx \left(\frac{\partial}{\partial x} e^{-k^2 x^2} \right)^2 = 4k^4 \int_{-\infty}^{\infty} dx x^2 e^{-k^2 x^2} = k \sqrt{\pi/2}. \quad (\text{A3})$$

Comparable integral identities exist when considering an ansatz proportional to $\text{sech}(kx)$. Thus:

$$\int_{-\infty}^{\infty} dx \text{sech}^2(kx) = \left[\frac{\tanh(kx)}{k} \right]_{-\infty}^{\infty} = \frac{2}{k}, \quad (\text{A4})$$

$$\int_{-\infty}^{\infty} dx \text{sech}^4(kx) = \left[\frac{\{\text{sech}^2(kx) + 2\} \tanh(kx)}{3k} \right]_{-\infty}^{\infty} = \frac{4}{3k}, \quad (\text{A5})$$

$$\begin{aligned} \int_{-\infty}^{\infty} dx \left[\frac{\partial}{\partial x} \text{sech}(kx) \right]^2 &= k^2 \int_{-\infty}^{\infty} dx \tanh^2(kx) \text{sech}^2(x) \\ &= \frac{k}{3} [\tanh(kx)]_{-\infty}^{\infty} = \frac{2k}{3}, \end{aligned} \quad (\text{A6})$$

all of which are necessary to determine the energy of a standard bright soliton solution to the nonlinear Schrödinger equation. However, we also require a contribution arising from the existence of an external harmonic confining potential. Hence, we determine

$$\begin{aligned} \int_{-\infty}^{\infty} dx x^2 \text{sech}^2(kx) &= 2 \int_0^{\infty} dx x^2 \text{sech}^2(kx) \\ &= \frac{2}{k^3} \left[\text{Li}_2(-e^{-2kx}) + kx \{ kx \tanh(kx) \right. \\ &\quad \left. - kx - 2 \ln(1 + e^{-2kx}) \} \right]_{0}^{\infty} \\ &= \frac{2}{k^3} [\text{Li}_2(0) - \text{Li}_2(-1)] \\ &= \frac{2}{k^3} \eta(2) = \frac{\pi^2}{6k^3}, \end{aligned} \quad (\text{A7})$$

where $\text{Li}_y(x) \equiv \sum_{n=1}^{\infty} x^n / n^y$ is a polylogarithm, and $-\text{Li}_y(-1) = \eta(y)$, the Dirichlet η function, with $\eta(2) = \pi^2/12$.

Appendix B: Solution to the quartic equations

We require a general solution to a quartic in ℓ of the form

$$\ell^4 + b\ell - c = 0, \quad (\text{B1})$$

where b and c are positive real constants, and ℓ must also take positive real values to be physically meaningful. This can be rephrased as the product of two quadratics in ℓ :

$$\left[\ell^2 + \alpha\ell + \frac{1}{2} \left(\alpha^2 - \frac{b}{\alpha} \right) \right] \left[\ell^2 - \alpha\ell + \frac{1}{2} \left(\alpha^2 + \frac{b}{\alpha} \right) \right] = 0, \quad (\text{B2})$$

so long as $(b^2/\alpha^2 - \alpha^4)/4 = c$. Hence, α , which remains to be determined, must solve $\alpha^6 + 4c\alpha^2 - b^2$.

Defining $\xi = \alpha^2$, the problem of determining α reduces to finding values of ξ to solve the depressed cubic equation

$$\xi^3 + 4c\xi - b^2 = 0. \quad (\text{B3})$$

Defining

$$A = \sqrt[3]{\frac{b^2}{2} + \sqrt{\frac{b^4}{4} + \frac{64c^3}{27}}}, \quad B = \sqrt[3]{\frac{b^2}{2} - \sqrt{\frac{b^4}{4} + \frac{64c^3}{27}}}, \quad (\text{B4})$$

the three roots of Eq. (B3) are given by:

$$\xi_1 = A + B, \quad (\text{B5})$$

$$\xi_2 = -(A + B)/2 + i\sqrt{3}(A - B)/2, \quad (\text{B6})$$

$$\xi_3 = -(A + B)/2 - i\sqrt{3}(A - B)/2. \quad (\text{B7})$$

Any one of these will solve Eq. (B3), however we choose ξ_1 ; as b and c are assumed positive real, ξ_1 is also conveniently guaranteed positive real.

Substituting in $\alpha = \sqrt{\xi_1}$, we can apply the quadratic formula to both the factors (enclosed in square brackets) on the

left hand side of Eq. (B2). This reveals the four roots to be

$$\ell_1 = \frac{-\sqrt{\xi_1} + \sqrt{-\xi_1 + 2b/\sqrt{\xi_1}}}{2}, \quad (\text{B8})$$

$$\ell_2 = \frac{-\sqrt{\xi_1} - \sqrt{-\xi_1 + 2b/\sqrt{\xi_1}}}{2}, \quad (\text{B9})$$

$$\ell_3 = \frac{\sqrt{\xi_1} + \sqrt{-\xi_1 - 2b/\sqrt{\xi_1}}}{2}, \quad (\text{B10})$$

$$\ell_4 = \frac{\sqrt{\xi_1} - \sqrt{-\xi_1 - 2b/\sqrt{\xi_1}}}{2}. \quad (\text{B11})$$

Recalling that b and ξ_1 are positive real, ℓ_3 and ℓ_4 are clearly complex, and therefore not of interest to us. Noting that

$$\xi_1^3 = A^3 + B^3 + 3AB(A + B) = b^2 - 4c\xi_1, \quad (\text{B12})$$

we can see that $A^3 + B^3 \equiv b^2 > \xi_1^3$, hence $4b^2 > \xi_1^3$ and thus $2b/\sqrt{\xi_1} > \xi_1$. Roots ℓ_1 and ℓ_2 are therefore real, but ℓ_2 is guaranteed negative. However, from Eq. (B12) it also follows that

$$b > \xi_1 \sqrt{\xi_1} \Rightarrow 2b/\sqrt{\xi_1} > 2\xi_1 \Rightarrow 2b/\sqrt{\xi_1} - \xi_1 > \xi_1 \\ \Rightarrow \sqrt{-\xi_1 + 2b/\sqrt{\xi_1}} > \sqrt{\xi_1}. \quad (\text{B13})$$

Hence ℓ_1 is guaranteed positive real, and is the only solution of interest.

Thus, the single positive real root of Eq. (B1) is

$$\ell = \frac{\chi^{1/2} b^{1/3}}{2^{7/6}} \left\{ \left[\left(\frac{2}{\chi} \right)^{3/2} - 1 \right]^{1/2} - 1 \right\}, \quad (\text{B14})$$

with

$$\chi = \left\{ 1 + \left[1 + \frac{(c/3)^3}{(b/4)^4} \right]^{1/2} \right\}^{1/3} + \left\{ 1 - \left[1 + \frac{(c/3)^3}{(b/4)^4} \right]^{1/2} \right\}^{1/3}, \quad (\text{B15})$$

and where values of all fractional powers are taken to be real, and positive when a positive root exists.

-
- [1] T. Dauxois and M. Peyrard, *Physics of Solitons* (Cambridge University Press, 2006).
 - [2] L. D. Fadeev and L. A. Takhtajan, *Hamiltonian Methods in the Theory of Solitons* (Springer-Verlag, Berlin, 1987).
 - [3] V. Zakharov and A. Shabat, Sov. Phys. JETP **34**, 62 (1972).
 - [4] J. Satsuma and N. Yajima, Prog. Theor. Phys. Suppl. **55**, 284 (1974).
 - [5] J. P. Gordon, Opt. Lett. **8**, 596 (1983).
 - [6] L. Khaykovich, F. Schreck, G. Ferrari, T. Bourdel, J. Cubizolles, L. D. Carr, Y. Castin, and C. Salomon, Science **296**, 1290 (2002).
 - [7] K. E. Strecker, G. B. Partridge, A. G. Truscott, and R. G. Hulet, Nature **417**, 150 (2002).

- [8] S. L. Cornish, S. T. Thompson, and C. E. Wieman, Phys. Rev. Lett. **96**, 170401 (2006).
- [9] L. Pitaevskii and S. Stringari, *Bose-Einstein Condensation* (Clarendon Press, Oxford, 2003).
- [10] V. M. Pérez-García, H. Michinel, J. I. Cirac, M. Lewenstein, and P. Zoller, Phys. Rev. Lett. **77**, 5320 (1996).
- [11] V. M. Pérez-García, H. Michinel, and H. Herrero, Phys. Rev. A **57**, 3837 (1998).
- [12] L. Salasnich, A. Parola, and L. Reatto, Phys. Rev. A **65**, 043614 (2002).
- [13] L. Salasnich, A. Parola, and L. Reatto, Phys. Rev. A **66**, 043603 (2002).
- [14] A. D. Martin, C. S. Adams, and S. A. Gardiner,

- Phys. Rev. Lett. **98**, 020402 (2007).
- [15] A. D. Martin, C. S. Adams, and S. A. Gardiner, Phys. Rev. A **77**, 013620 (2008).
 - [16] N. G. Parker, A. M. Martin, S. L. Cornish, and C. S. Adams, J. Phys. B **41**, 045303 (2008).
 - [17] N. G. Parker, A. M. Martin, C. S. Adams, and S. L. Cornish, Physica D **238**, 1456 (2009).
 - [18] T. P. Billam, S. L. Cornish, and S. A. Gardiner, Phys. Rev. A **83**, 041602(R) (2011).
 - [19] D. Poletti, E. A. Ostrovskaya, T. J. Alexander, B. Li, and Y. S. Kivshar, Physica D **238**, 1338 (2009).
 - [20] S. L. Cornish, N. G. Parker, A. M. Martin, T. E. Judd, R. G. Scott, T. M. Fromhold, and C. S. Adams, Physica D **238**, 1299 (2009).
 - [21] L. Khaykovich and B. A. Malomed, Phys. Rev. A **74**, 023607 (2006).
 - [22] U. Al Khawaja, H. T. C. Stoof, R. G. Hulet, K. E. Strecker, and G. B. Partridge, Phys. Rev. Lett. **89**, 200404 (2002).
 - [23] K. E. Strecker, G. B. Partridge, A. G. Truscott, and R. G. Hulet, N. J. Phys. **5**, 73 (2003).
 - [24] L. D. Carr and J. Brand, Phys. Rev. Lett. **92**, 040401 (2004).
 - [25] B. J. Dąbrowska-Wüster, S. Wüster, and M. J. Davis, N. J. Phys. **11**, 053017 (2009).
 - [26] U. Al Khawaja and H. T. C. Stoof, N. J. Phys. **13**, 085003 (2011).
 - [27] C. Weiss and Y. Castin, Phys. Rev. Lett. **102**, 010403 (2009).
 - [28] A. I. Streltsov, O. E. Alon, and L. S. Cederbaum, Phys. Rev. Lett. **99**, 030402 (2007).
 - [29] A. I. Streltsov, O. E. Alon, and L. S. Cederbaum, Phys. Rev. A **80**, 043616 (2009).
 - [30] A. D. Cronin, J. Schmiedmayer, and D. E. Pritchard, Rev. Mod. Phys. **81**, 1051 (2009).
 - [31] J. A. Dunningham and K. Burnett, Phys. Rev. A **70**, 033601 (2004).
 - [32] J. A. Dunningham, Contemp. Phys. **47**, 257 (2006).
 - [33] A. B. Tacla and C. M. Caves, Phys. Rev. A **84**, 053606 (2011).
 - [34] N. G. Parker, S. L. Cornish, C. S. Adams, and A. M. Martin, J. Phys. B **40**, 3127 (2007).
 - [35] P. A. Ruprecht, M. J. Holland, K. Burnett, and M. Edwards, Phys. Rev. A **51**, 4704 (1995).
 - [36] J. L. Roberts, N. R. Claussen, S. L. Cornish, E. A. Donley, E. A. Cornell, and C. E. Wieman, Phys. Rev. Lett. **86**, 4211 (2001).
 - [37] E. A. Donley, N. R. Claussen, S. L. Cornish, J. L. Roberts, E. A. Cornell, and C. E. Wieman, Nature **412**, 295 (2001).
 - [38] J. M. Gerton, D. Strekalov, I. Prodan, and R. G. Hulet, Nature **408**, 692 (2000).
 - [39] L. P. Pitaevskii, Physics Letters A **221**, 14 (1996).
 - [40] C. M. Savage, N. P. Robins, and J. J. Hope, Phys. Rev. A **67**, 014304 (2003).
 - [41] P. A. Altin, G. R. Dennis, G. D. McDonald, D. Döring, J. E. Debs, J. D. Close, C. M. Savage, and N. P. Robins, Phys. Rev. A **84**, 033632 (2011).
 - [42] A. Gammal, T. Frederico, and L. Tomio, Phys. Rev. A **64**, 055602 (2001).
 - [43] A. Gammal, L. Tomio, and T. Frederico, Phys. Rev. A **66**, 043619 (2002).
 - [44] A. M. Kamchatnov and V. S. Shchesnovich, Phys. Rev. A **70**, 023604 (2004).
 - [45] L. D. Carr and Y. Castin, Phys. Rev. A **66**, 063602 (2002).
 - [46] V. I. Yukalov and E. P. Yukalova, Phys. Rev. A **72**, 063611 (2005).
 - [47] S. A. Morgan, Phys. Rev. A **72**, 043609 (2005).
 - [48] Y. Lai and H. A. Haus, Phys. Rev. A **40**, 854 (1989).